OPTICAL PHASE DISTORTION DUE TO COMPRESSIBLE FLOW OVER LASER TURRETS

by

Allen E. Fuhs
Distinguished Professor
Naval Postgraduate School
Monterey, California, 93940

and

Susan E. Fuhs
Student, Chemical Engineering
California Institute of Technology
Pasadena, California, 91125,

ABSTRACT

Compressible flow over a laser turret causes variation in density and the index of refraction. As a result, a laser beam develops a phase distortion. Phase distortion has been calculated for both blunt and small perturbation turrets. For the blunt turret, the Janzen-Rayleigh technique was used to determine the flow field. Phase distortions of 2.2 wavelengths at 3.8 microns were calculated for the blunt turret. For small perturbation turrets a versatile analytical model was developed for a turret on a fuselage with circular cross section. With a two-dimensional Fourier series representation of the turret, any shape can be considered. Both subsonic and supersonic flows can be calculated. Phase distortions of 1.2 wavelengths at 3.8 microns were calculated for one turret at high subsonic Mach number. In addition to being of value for laser turrets, the methods are applicable to reconnaissance aircraft using photographic equipment and cruise missiles using celestial navigation.

INTRODUCTION

Large scale laser telescopes are being installed aboard aircraft [1, 2]. Airflow over the laser turret causes density variations. Since the index of refraction depends on density, a phase distortion is generated as the beam

propagates outward from the laser telescope. A phase distortion may tilt, defocus, or focus the beam. Higher-order aberrations, such as astigmatism and coma, may also occur.

Denote the characteristic geometric scale of the laser turret by ℓ. The diameter of the telescope aperture is D. The ratio D/ℓ tends to be much greater for laser installations than for other optical devices commonly installed on board aircraft. As an example, consider the pilot's eye. For this case, ℓ is the size of the canopy, and D is several millimeters. The pilot does not experience optical distortion due to the small value of D/ℓ.

Laser turrets tend to differ from camera installations aboard reconnaissance aircraft [3]. Due to the large size of D and the desire to have wide angular coverage, laser turrets protrude into the airstream. Camera installations usually have flat windows which are flush mounted in the fuselage. Furthermore, camera apertures may be considerably less than laser apertures. As a result of these two facts, degradation of photographic image quality usually is not a serious problem. However, in the event of image degradation, the methods of this paper could be applied to remove distortions.

Cruise missiles with intercontinental ranges may use celestial navigation which requires precise measurement of angular location of stars. A distorted lens created by the ambient flow field causes an error in measurement. Knowledge of the external aerodynamics is important [3].

Optical distortion due to the external flow field can be divided into two categories [4]. Viscous flow phenomena fall into one category and include shear layers, laminar and turbulent boundary layers, and the shedding of discrete vortices. The other category involves the external inviscid flow field. Based on the preceding discussion, the reader recognizes that this paper treats the latter category.

Laser turrets can be classified as either blunt or small perturbation turrets. If a turret has a surface with a normal vector, $\vec{n}$, aligned parallel or nearly so, to the freestream velocity vector, $\vec{V}_\infty$, the turret is "blunt." If the angle between the normal vectors of the turret surface and the free-stream velocity is everywhere large, e.g., 60° to 90°, then the turret is "small-perturbation." Both types of laser turrets are discussed in this paper.

BACKGROUND INFORMATION

Critical Mach Number

A useful concept is the critical Mach number, M_∞^*. At the critical Mach number, somewhere on the body a local Mach number is sonic. When $M_\infty > M_\infty^*$, the flow becomes inherently nonlinear and shock waves appear. The transonic flow equations must be solved when $M_\infty \cong M_\infty^*$. The occurrence of shock waves usually implies severe degradation of the laser beam quality.

The critical Mach numbers for several body geometries are listed in Table I. One advantage of the solution developed later in this paper is the fact that the critical Mach number can be calculated. Results are shown in Table I for a cosine shaped turret which will be discussed in more detail in the section Turret on a Circular Fuselage: Subsonic Flow.

Laser Turret Map

Different analytical models must be developed for different laser turret geometries. A map can be drawn showing the various flow regions for the different turret geometries. Figure 1 is a laser turret map. The abscissa is the freestream Mach number, M_∞. The ordinate is the maximum slope of the turret. Various regions are defined by capital letters.

The flow within region ABCD can be described with sufficient accuracy using the linearized small perturbation equations. The line CD represents the

Table I. Critical Mach Numbers for Several Geometric Shapes

Body Shape	Ratio ε/R_0	Critical Mach Number
Circular cylinder with axis normal to flow [5]	–	0.3985
Sphere [5]	–	0.5868
Hemisphere-cylinder with cylinder axis parallel to flow [6,7]	–	< 0.7
Cosine shaped turret on circular fuselage [3]	0.05	0.88
	0.10	0.82
	0.15	0.76
	0.20	0.72
	0.25	0.68
	0.30	0.65

ε = amplitude or maximum height of turret

R_0 = radius of circular fuselage

turret length/fuselage radius ratio = 1.005

critical Mach number. The line BC is shown at a slope of 30°. The assumptions involved in the linearization of the potential flow equation become less and less valid as the maximum slope increases. The region CDJ, which resembles an inverted triangle, requires solution of the nonlinear, small perturbation, transonic, potential flow equation.
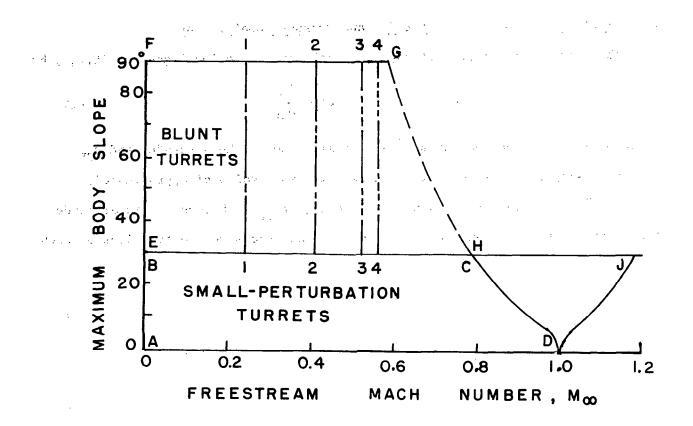
Figure 1. Freestream Mach Number Regions for Application of Various Analytical
Models.

EFGH defines the region where the solution to the blunt-body nonlinear flow

equations is necessary. The line GH, which defines the critical Mach number, is

shown dashed; the critical Mach number is a function of turret shape. Hence GH

is intended to suggest qualitatively the upper bound for Mach number for

blunt turrets. Within region EFGH the Janzen-Rayleigh [5,8,9,10] technique is

most useful.

Vertical lines 1, 2, 3, and 4 occur within region EFGH. These lines

represent the upper bound of applicability of the first, second, third, and

fourth-order solutions when the Janzen-Rayleigh technique is used. The first-

order solution may be applied with region F11E; the second-order solution, within

F22E; etc. The hemispherical turret considered in the following section is an

example of a turret falling along line FG.

Phase Distortion, Index of Refraction and Pressure Coefficient

The local index of refraction, n, is related to the local gas density, ρ, by

$$n = 1 + \kappa \frac{\rho}{\rho_\infty} = 1 + \kappa' \frac{\rho}{\rho_\infty} \frac{\rho_\infty}{\rho_{SL}} \tag{1}$$

where ρ_∞ is the freestream density at the altitude of the aircraft, and ρ_{SL} is the density at sea level. The constant κ' has a value of approximately 2.3×10^{-4} in the infrared. Note that $\kappa = \kappa'(\rho_\infty / \rho_{SL})$; obviously κ is altitude dependent. Assuming isentropic flow, density and pressure are functions of each other

$$p/p_\infty = (\rho/\rho_\infty)^\gamma \tag{2}$$

Using the definition of pressure coefficient, C_p, one can show that

$$\frac{p}{p_\infty} = 1 + \frac{\gamma M_\infty^2 C_p}{2} \tag{3}$$

In equations (2) and (3) γ is the ratio of heat capacities, and M_∞ is the freestream Mach number. Combining equations (1) to (3) yields

$$n = 1 + \kappa' \frac{\rho_\infty}{\rho_{SL}} \left(1 + \frac{\gamma M_\infty^2 C_p}{2} \right)^{1/\gamma} \tag{4}$$

Since C_p may be positive or negative, n may be increased or decreased by the flow.

Optical path length, L, is defined as

$$L_i = \int_a^b n(s) \, ds \tag{5}$$

where s is the distance along a ray, and points a and b are positioned on the ray. The index of refraction n is a function of s. The subscript i identifies a particular ray within the laser beam. The difference in optical path length between two rays i and j is

$$\Delta L = L_j - L_i = \int_a^b [n(s_j) - n(s_i)]ds \tag{6}$$

The optical path length has the dimensions of length, e.g., meter; to make L nondimensional, the wavelength of radiation, λ, can be used as a reference. The ratio $\Delta L/\lambda$ is known as the phase distortion P. Combining equations (4) and (6) gives a formula for P,

$$P = \frac{\kappa'}{\lambda} \frac{\rho_\infty}{\rho_{SL}} R_0 \int_0^\infty \left[\left(1 + \frac{\gamma M_\infty^2 C_p}{2}\right)_j^{\frac{1}{\gamma}} - \left(1 + \frac{\gamma M_\infty^2 C_p}{2}\right)_i^{\frac{1}{\gamma}} \right] d\left(\frac{s}{R_0}\right) \tag{7}$$

Equation (7) shows the dependence on altitude. The solutions for the various flow fields give values of C_p.

Zernike Polynomials

A wavefront shape or the same thing, the phase distortion, can be expressed in terms of Zernike polynomials [11]. Equations (8) through (17) can be found in the paper by Hogge and Butts [12].

$$F_1(r) = \left(\frac{1}{\pi R^2}\right)^{1/2}, \quad \text{(uniform phase shift)} \tag{8}$$

$$F_2(r) = \left(\frac{4}{\pi R^4}\right)^{1/2} x, \quad \Big\} \quad \text{(tilt)} \tag{9}$$

$$F_3(r) = \left(\frac{4}{\pi R^4}\right)^{1/2} y, \tag{10}$$

$$F_4(r) = \left(\frac{12}{\pi R^6}\right)^{1/2} \left(x^2 + y^2 - \frac{R^2}{2}\right), \quad \text{(refocus)} \tag{11}$$

$$F_5(r) = \left(\frac{6}{\pi R^6}\right)^{1/2} (x^2 - y^2), \quad \Big\} \quad \text{(astigmatism)} \tag{12}$$

$$F_6(r) = \left(\frac{24}{\pi R^6}\right)^{1/2} (xy), \tag{13}$$

$$F_7(r) = \left(\frac{8}{\pi R^8}\right)^{1/2} (x^3 - 3xy^2), \qquad \text{(14)}$$

$$F_8(r) = \left(\frac{8}{\pi R^8}\right)^{1/2} (y^3 - 3yx^2), \qquad \text{(15)}$$

$$F_9(r) = \left(\frac{8}{\pi R^8}\right)^{1/2} (3x^2 + 3y^2 - 2R^2)x, \qquad \text{(coma)} \qquad \text{(16)}$$

$$F_{10}(r) = \left(\frac{8}{\pi R^6}\right)^{1/2} (3x^2 + 3y^2 - 2R^2)y. \qquad \text{(17)}$$

The Zernike polynomials are an orthonormal set of functions over an aperture of radius R. The phase distortion can be represented as

$$P = \sum_{j=1}^{10} A_j F_j(r) \qquad \text{(18)}$$

where A_j is a constant which characterizes the phase distortion P. A_j is given by

$$A_j = \int_0^{2\pi} \int_0^R P(r,\theta) F(r,\theta) r \, dr \, d\theta \qquad \text{(19)}$$

In equation (19) one could have used x and y as variables; however, use of θ and r is more appropriate for a circular aperture.
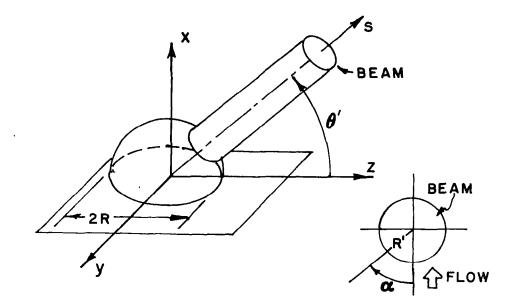
Since the Zernike polynomials are related to the various aberrations, knowledge of the coefficients A_j indicates the magnitude of each aberration [12]. Further, the values of A_j are helpful for designing adaptive optics systems to overcome partially the aberrations.
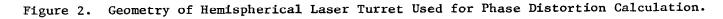
BLUNT LASER TURRET

As an example of phase distortion due to compressible flow over a blunt turret, a hemispherical turret was selected [13,14]. Another shape amenable to analytical solution would be an ellipsoidal turret.

Janzen-Rayleigh Solution

The geometry is shown in Figure 2. A beam of radius R'_b is propagated from a turret of radius R. The elevation of the beam above the y-z plane is θ'. Distance along the beam is s. Points within a plane normal to the beam are located by coordinates R' and α. The windward and leeward sides of the laser beam can be determined from the flow arrow.

Figure 2. Geometry of Hemispherical Laser Turret Used for Phase Distortion Calculation.

In spherical coordinates, the equations of motion are as follows:

$$u\frac{\partial u}{\partial r} + \frac{v}{r}\frac{\partial u}{\partial \theta} - \frac{v^2}{r} = -\frac{1}{\rho}\frac{\partial p}{\partial r} = -\frac{a^2}{\rho}\frac{\partial \rho}{\partial r} \qquad (20)$$

$$u\frac{\partial v}{\partial r} + \frac{v}{r}\frac{\partial v}{\partial \theta} + \frac{uv}{r} = -\frac{1}{\rho r}\frac{\partial p}{\partial \theta} = -\frac{a^2}{\rho r}\frac{\partial \rho}{\partial \theta} \qquad (21)$$

$$\frac{1}{\rho}(u\frac{\partial \rho}{\partial r} + \frac{v}{r}\frac{\partial \rho}{\partial \theta}) + \frac{1}{r^2}\frac{\partial}{\partial r}(r^2 u) + \frac{1}{r\sin\theta}\frac{\partial}{\partial \theta}(v\sin\theta) = 0 \qquad (22)$$

Equations (20) and (21) are Euler's equations; equation (22) is the continuity equation. For flow over a sphere, the azimuth angle is not a dependent variable. Multiplying equation (20) by $+ u/a^2$ and equation (21) by $- v/a^2$, adding, and combining with equation (22) yields

$$\frac{1}{r^2} \frac{\partial}{\partial r}(r^2 u) + \frac{1}{r \sin \theta} \frac{\partial}{\partial \theta} (v \sin \theta) = \frac{1}{a^2}\left(u^2 \frac{\partial u}{\partial r} + \frac{uv}{r} \frac{\partial v}{\partial \theta} + uv \frac{\partial v}{\partial r} + \frac{v^2}{r} \frac{\partial v}{\partial \theta}\right) \quad (23)$$

The speed of sound, a, is the local value and changes from point to point in the flow. Variations in a must be accounted for. Using the energy equation along a streamtube, one can show that

$$\frac{a^2}{a_\infty^2} = 1 + \frac{\gamma - 1}{2} M_\infty^2\left(1 - \frac{u^2 + v^2}{U^2}\right) \quad (24)$$

Inviscid flow is considered. A potential function, ϕ, can be introduced for the velocity components

$$u = U \frac{\partial \phi}{\partial r} \quad (25)$$

and

$$v = \frac{U}{r} \frac{\partial \phi}{\partial \theta} \quad (26)$$

Combining equations (23) to (26) yields an equation in which the only dependent variable is ϕ.

The Rayleigh-Janzen expansion considers the potential function to be given as

$$\phi = \phi_0 + M_\infty^2 \phi_1 + M_\infty^4 \phi_2 + \ldots \quad (27)$$

The solution ϕ_0 is considered to be the first-order solution; the solution involving both ϕ_0 and ϕ_1 is termed the second-order solution. In this paper only the first and second-order solutions are discussed. For ease of writing, the following definition is introduced:

$$\psi = M_\infty^2 \phi_1 \quad (28)$$

Substitution of ψ into the potential equation gives

$$\nabla^2\phi_0 + \nabla^2\psi = M_\infty^2\left(\phi_r\phi_{rr} + \frac{2}{r^2}\phi_r\phi_\theta\phi_{\theta r} - \frac{1}{r^3}\phi_\theta^2\phi_r + \frac{1}{r^4}\phi_\theta^2\phi_{\theta\theta}\right) \tag{29}$$

where __all__ terms on the right-hand side are determined from the first-order

potential function, ϕ_0. The result of equating coefficients of like powers in M_∞^2

yields two equations

$$\nabla^2\phi_0 = 0 \tag{30}$$

and

$$\nabla^2\psi = M_\infty^2\nabla^2\phi_1 = M_\infty^2\left(\phi_r^2\phi_{rr} + \frac{2}{r^2}\phi_r\phi_\theta\phi_{r\theta} - \frac{1}{r^3}\phi_\theta^2\phi_r + \frac{1}{r^4}\phi_\theta^2\phi_{\theta\theta}\right) \tag{31}$$

Equation (31) is Poisson's equation.

The first-order solution can be obtained from Milne-Thompson [15], Lamb [16],
or Karamcheti [17]. It is

$$\phi_0 = U\left(r\cos\theta + \frac{R^3\cos\theta}{2r^2}\right) \tag{32}$$

Equation (32) can be used to evaluate the right-hand side of equation (29).

In July, 1916, Lord Rayleigh [10] reported the solution for the second-order
function. The Legendre functions

$$P_1 = \cos\theta \tag{33}$$

and

$$P_3 = \frac{5}{3}\cos^3\theta - \frac{3}{2}\cos\theta \tag{34}$$

are introduced into equation (31). The result is

$$\nabla^2\phi_1 = \frac{U}{2}\left[\left(-\frac{36}{5}\frac{R^6}{r^7} + \frac{9}{2}\frac{R^9}{r^{10}}\right)P_1 + \left(6\frac{R^3}{r^4} - \frac{24}{5}\frac{R^6}{r^7} + \frac{3}{2}\frac{R^9}{r^{10}}\right)P_3\right] \tag{35}$$

Using the defining equation for the Legendre function, equation (35) can be solved to yield

$$\phi = \phi_0 + M_\infty^2 \phi_1 = \left[U\left(r + \frac{R^3}{2r^2}\right)P_1\right] + UM_\infty^2\left[\left(\frac{R^3}{3r^2} - \frac{R^6}{5r^5} + \frac{R^9}{24r^8}\right)P_1\right.$$

$$\left. + \left(-\frac{3R^3}{10r^2} + \frac{27R^5}{55r^4} - \frac{3R^6}{10r^5} + \frac{3R^9}{176r^8}\right)P_3\right] \tag{36}$$

Equation (36) can be inserted into equations (25) and (26) to find u and v. Knowing u and v, equation (24) can be evaluated. To evaluate equation (1) for n, one needs ρ/ρ_∞. Since the flow is isentropic

$$\frac{\rho}{\rho_\infty} = \left(\frac{1 + \frac{\gamma - 1}{2}M_\infty^2}{1 + \frac{\gamma - 1}{2}M^2}\right)^{\frac{1}{\gamma-1}} \tag{37}$$

The local Mach number is given by

$$M^2 = \frac{1}{a^2}\left[\left(\frac{\partial\phi}{\partial r}\right)^2 + \left(\frac{1}{r}\frac{\partial\phi}{\partial\theta}\right)^2\right] \tag{38}$$

Combining equations (1) and (36) through (38) with equation (5) allows calculation of the optical path length.

Geometry for Calculating Phase Distortion

Refer once again to Figure 2. The flow properties, e.g., density and Mach number, are functions of r and θ. These are polar coordinates. Consequently it is necessary to express r and θ in terms of θ', s, α, and R'. The equations are

$$r^2 = [(R + s)\sin\theta' - R'\cos\alpha\cos\theta']^2 + R'^2\sin^2\alpha$$

$$+ [(R + s)\cos\theta' + R'\cos\alpha\sin\theta']^2 \tag{39}$$

and

$$\theta = \tan^{-1}\frac{\sqrt{[(R + s)^2\sin^2\theta' - R'\cos\alpha\cos\theta']^2 + R'^2\sin^2\alpha}}{[(R + s)\cos\theta' + R'\cos\alpha\sin\theta']} \tag{40}$$

298

Equations (39) and (40) allow calculation of independent variables for the flow in terms of a location in the laser beam as specified by s, R', α, and θ'.

Figure 3 illustrates the distance along the beam, s, and the gap which exists between the surface of the turret and the s = 0 plane. The phase distortion is given by
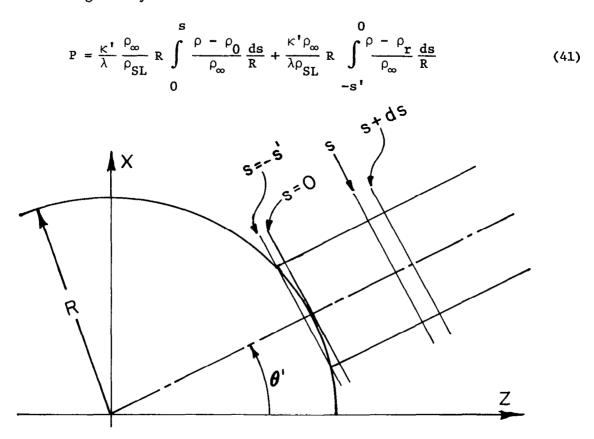
$$P = \frac{\kappa'}{\lambda} \frac{\rho_\infty}{\rho_{SL}} R \int_0^s \frac{\rho - \rho_0}{\rho_\infty} \frac{ds}{R} + \frac{\kappa'\rho_\infty}{\lambda\rho_{SL}} R \int_{-s'}^0 \frac{\rho - \rho_r}{\rho_\infty} \frac{ds}{R} \qquad (41)$$

Figure 3. Cross Section of Turret and Beam in x-z Plane.

where ρ_0 is the density along the axis of the beam and ρ_r is a reference density. The second integral in equation (41) has been termed the "gap integral."

Graphical Presentation of Results

A computer program has been developed for the HP9830 which calculates the phase distortion, P, as a function of sphere radius, R; elevation angle, θ'; radius within the beam, R'; angle within the beam, α; freestream Mach number, M_∞; wavelength, λ; index of refraction constant, κ'; ratio of heat capacities, γ; freestream speed of sound, a_∞; and density ratio, ρ_∞/ρ_{SL}. Values used in the

calculations are as follows:

$$\text{beam diameter} = R/2 = 0.4572 \text{ meter}$$

$$R = 0.9144 \text{ meter}$$

$$\lambda = 3.8 \times 10^{-6} \text{ meter}$$

$$\kappa' = 2 \times 10^{-4}$$

$$a = 342 \text{ meters/sec}$$

$$\gamma = 1.4$$

$$\rho_\infty / \rho_{SL} = 1.0$$

M_∞, R', α, and θ' have been varied. Calculations have been performed to the extent necessary to plot phase distortion maps.

Plots of isocontours of phase shift were made for steps of 18° starting with $\theta' = 0$ and $\theta' = 90^\circ$. The calculations ignore the gap integral; evaluation of gap integral is somewhat arbitrary. However, to provide insight to the magnitude of the gap integral, the quantity was evaluated with $\rho_r = \rho_\infty$ in equation (41). Results are shown in Table II.

Table II. Maximum Value of Gap Integral

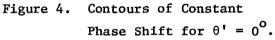| Beam Elevation Angle θ'	Maximum Value of Gap Integral and Location Within Beam	
0	0.368	*
18	0.654	0°
36	0.678	0°
54	-0.836	180°
72	-0.863	120°
90	-0.866	90°

*Does not depend on α.

The quantity, maximum value of gap integral, is the maximum phase distortion, P, caused by the gap between the plane s = 0 and the surface of the turret. From Table II, the large value of the gap integral indicates that the gap cannot be ignored.

The plots of isocontours of phase shift are shown in Figures 4 to 9. To avoid awkward decimal values, the phase distortion has been multiplied by 100. Hence 250 from the graphs is 2.5 wavelengths phase distortion; a value of 25 from the curves would be a quarter wavelength. Recall the beam axis is used as the reference for the phase shift, P. Reference to equation (41) shows that P is positive when ρ along the ray in question exceeds ρ_∞. A positive value of P means the wavefront lags behind the front at the beam axis.

The critical Mach number 0.587 was chosen for the calculations. The outer edge of each plot is, of course, the outer edge of the beam. The ratio of turret diameter to beam diameter is 4.0. The significance of the maps will be discussed in the following subsection.
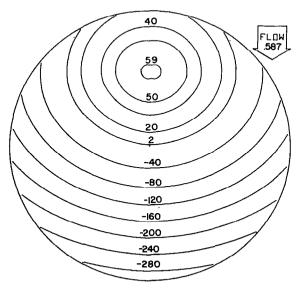

Figure 4. Contours of Constant
Phase Shift for $\theta' = 0°$.

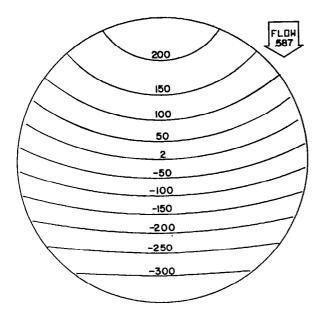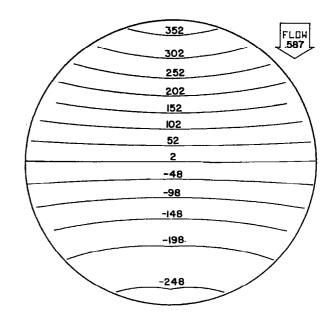Figure 5. Contours of Constant
Phase Shift for $\theta' = 18°$.

Figure 6.   Contours of Constant
            Phase Shift for $\theta' = 36°$.

Figure 7.   Contours of Constant
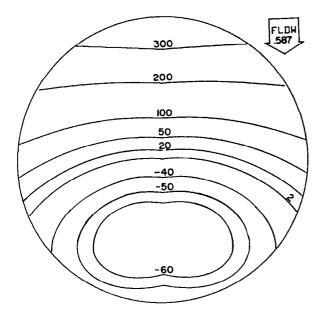   Phase Shift for $\theta' = 54°$.

Figure 8.   Contours of Constant
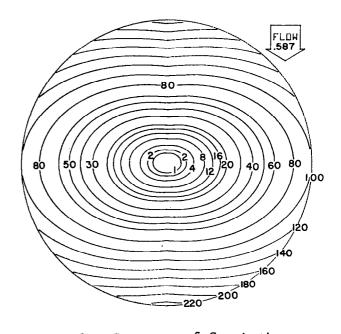   Phase Shift for $\theta' = 72°$.

Figure 9.   Contours of Constant
            Phase Shift for $\theta' = 90°$.

An important question is the rate of decay of the integrand in equation (41).
Calculations were made of

$$\frac{\partial P}{\partial (s/R)}$$

which is the phase distortion per unit distance along the beam. Results of the
calculation are shown in Figure 10. The phase distortion, P, is the area
enclosed by one of the curves. Most of the phase distortion occurs within a
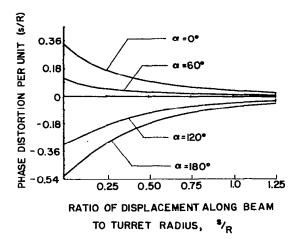distance of one turret radius.

Figure 10. Phase Distortion per Unit (s/R) as a Function of (s/R) for Rays
at $\alpha = 0^{\circ}$, 60°, 120°, and 180° Within the Beam. Elevation angle was
$\theta' = 18^{\circ}$.

The windward side of the beam is at $\theta = 0^{\circ}$. When $\theta' = 18$ and $\theta = 0$, the
air is compressed and P is positive. When $\theta = 180^{\circ}$, i.e., on the leeward side
of the beam, the air is expanded and P is negative.

Interpretation of Results

The contours in Figure 4 are a series of concentric circles with a negative
value of phase shift. Hence, the beam is being focused. The focal length, F, can
be estimated from

$$F = \frac{R_b'^2}{\lambda P} \tag{42}$$

Using $R_b' = R/4 = 0.2286$ meter, $\lambda = 3.8$ micron, and $P = 1.6$, the value of F is 8.6 km.

For $\theta' = 54°$ in Figure 7, the contours are almost straight lines. The algebraic signs of phase shift indicate the beam is being tilted in a direction opposite to the relative wind, i.e., the beam is leaning into the wind. The tilt angle is given by

$$\text{(tilt angle)} = \lambda \frac{\partial P}{\partial R'} \tag{43}$$

Inserting values from Figure 7, the tilt angle is found to be 26.5 microradians. This tilt angle should be compared with the pointing accuracy of the pointer-tracker which forms the turret. Fortunately tilt can be corrected easily by adaptive optics.

For $\theta' = 90°$, the flow over the turret causes defocusing of the beam; see Figure 9. Using equation (42), the focal length is $F = -6.3$ km. The flow gives effectively a negative lens.

Scaling of Phase Distortion

Using equation (41) one can demonstrate the scaling relationships for altitude (density), turret size, and laser wavelength. The equation is

$$\frac{P_2}{P_1} = \frac{\lambda_1}{\lambda_2} \frac{\rho_2}{\rho_1} \frac{R_2}{R_1} \frac{\kappa_2'}{\kappa_1'} \tag{44}$$

where subscripts 1 and 2 refer to two different hemispherical turrets at the same M_∞. The phase distortion becomes more severe as wavelength decreases. Throughout the infrared region, the value of κ' is nearly constant; however, as one approaches the visible, κ' tends to increase with decreasing wavelength. Of course, for constant diffraction, the ratio R/λ will tend to be constant. Since ρ follows an exponential decay with altitude, the phase distortion falls rapidly with increasing altitude.

TURRET ON A CIRCULAR CROSS SECTION FUSELAGE: SUBSONIC FLOW

Using the solution for the wavy wall on a cylinder [18] and Fourier

analysis, a turret of any shape can be described mathematically, and the flow

field can be obtained. A question about this model concerns the effect of fuselage

ends.

Fuselage End Effects

For the analytical model to apply, the fuselage shown in Figure 11 must extend

to infinity in both directions. Obviously real aircraft have finite length. What

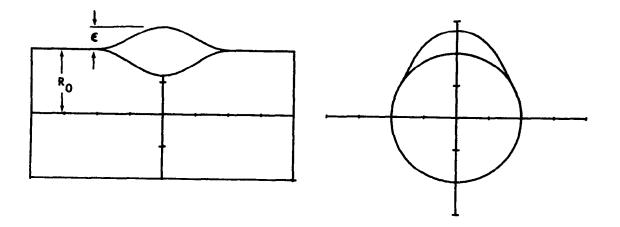is the influence of aircraft fuselage ends?

Figure 11. A Small Perturbation Turret on a Circular Cross Section Fuselage.

To gain insight to this question, the pressure distribution on the surface

of several axisymmetric bodies has been calculated assuming potential flow. The

fineness ratio of the fuselage, i.e., the ratio of length to diameter, was varied.

The potential equation for axisymmetric flow is

$$\frac{\partial^2 \phi'}{\partial z'^2} + \frac{1}{r'} \frac{\partial}{\partial r'}(r' \frac{\partial \phi'}{\partial r'}) = 0 \qquad (45)$$

where z' is distance in the flow direction and r' is radial distance using cylindrical coordinates. Equation (45) assumes incompressible flow although the calculated flow may be accurate to $M_\infty = 0.3$, depending on body bluntness.

A body surface is generated by a source-sink combination separated by a distance ℓ. Lengths are made nondimensional using ℓ. The potential function is nondimensionalized by the following

$$\phi = \phi'/U_\infty \ell \qquad (46)$$

where U_∞ is the freestream velocity.

There are two other lengths in the problem in addition to ℓ. First, there is the body diameter. Second, there is the distance from the source to the upstream stagnation point which is designated as z*. Once again z* is a nondimensional length using ℓ as a reference. Incidentally, the upstream and downstream stagnation points are saddle point singularities; this is a fact to be remembered when the equations are integrated to obtain the body surface.

The velocity components are $u = u'/U_\infty$ in the z-direction, and $v = v'/U_\infty$ in the r-direction. The equations for u and v are as follows:

$$u = 1 + \frac{z^{*2}(z^* - 1)^2 z}{(1 - 2z^*)(z^2 + r^2)^{3/2}} - \frac{z^{*2}(z^* - 1)^2(z - 1)}{(1 - 2z^*)[(z - 1)^2 + r^2]^{3/2}} \qquad (47)$$

and

$$v = \frac{z^{*2}(z^* - 1)^2 r}{(1 - 2z^*)(z^2 + r^2)^{3/2}} - \frac{z^{*2}(z^* - 1)r}{(1 - 2z^*)[(z - 1)^2 + r^2]^{3/2}} \qquad (48)$$

The flow is in the direction of the positive z axis with the source at z = 0 and the sink at z = 1. Consequently, the upstream stagnation point occurs at a location where z* is a negative number. When z* approaches negative infinity, the body approaches a sphere. When z* approaches zero, the length of the fuselage, which is $L = \ell(1 + 2z^*)$, approaches infinity. Any value of z*

satisfies equation (47) when u = 0 (a stagnation point), z = z*, and r = 0.

However different values of z* change the length to diameter ratio of the body.

To find the body surface, the differential equation relating velocity

components and the slope of the body surface is solved numerically; the equation

to be solved is

$$\frac{dr}{dz} = \frac{u}{v} \qquad\qquad (49)$$

Integration starts at $z = - |z*|$ and $r = 0$. Since the rear stagnation point is a

saddle point singularity, one cannot integrate to $z = + |z*|$ and $r = 0$. The flow

is known to be symmetric relative to z = 0.5; this fact was used to obtain the body

for z > 0.5.

The pressure coefficient in terms of nondimensional velocities is

$$C_p = \frac{p - p_\infty}{\rho U_\infty^2/2} = 1 - u^2 - v^2 \qquad\qquad (50)$$
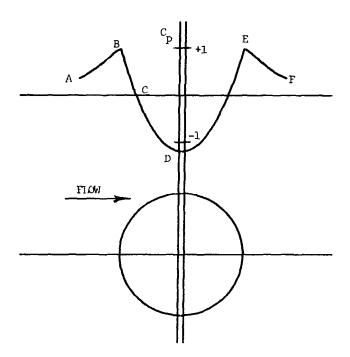
At the front and rear stagnation points, C_p has a value of unity. When C_p is zero,

the local static pressure exactly equals the static pressure at infinity, and

the local flow velocity is U_∞. When C_p is negative, the local flow velocity

exceeds U_∞.

Results of sample calculations are shown graphically in Figures 12 to 17.

In Figure 12 the length to diameter ratio, L/D, is 1.004, which is nearly a sphere.

The curves from A to B and from E to F are the pressure coefficient along the

stagnation streamlines. The curve BCDE is C_p on the surface of the body. For a

sphere, the pressure coefficient is

$$C_p = 1 - \frac{9}{4} \sin^2\theta \qquad\qquad (51)$$

When $\theta = 90^\circ$, $C_p = - 5/4$. When $\theta = 41.8^\circ$, $C_p = 0$, which corresponds to point C in

Figure 12.

For all figures, the sharp positive peaks are at $C_p = + 1.0$. Note that for

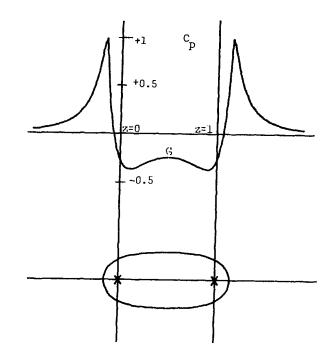L/D = 1.004, the C_p curve for the body surface is concave. For L/D = 2, the C_p

307

Figure 12. Pressure Coefficient on
Stagnation Streamline
and Body Surface.
$L/D = 1.004$

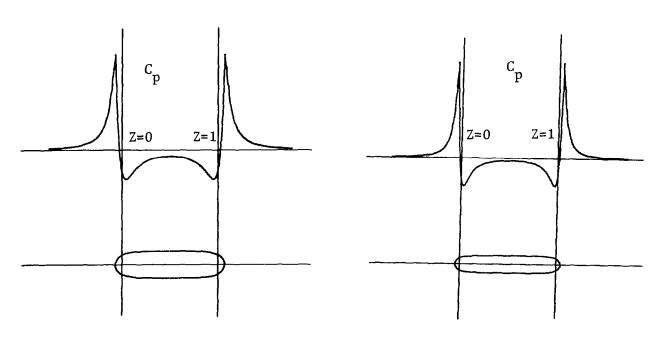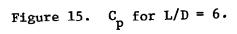Figure 13. C_p for $L/D = 2$. (The x's are
the source and sink.)

Figure 14. C_p for $L/D = 4$.
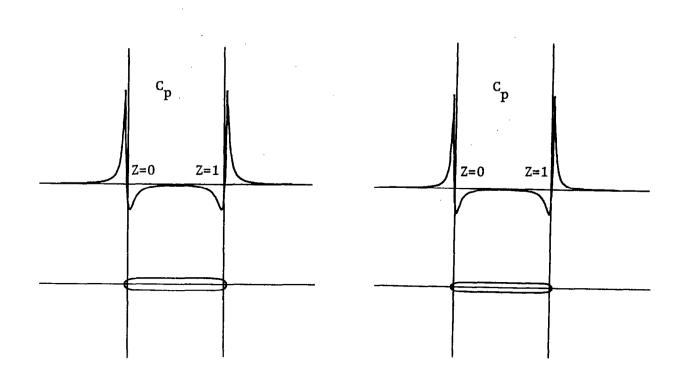

Figure 15. C_p for $L/D = 6$.

Figure 16. C_p for L/D = 8.   Figure 17. C_p for L/D = 10.

curve is convex at z = 0.5; this is point G in Figure 13. Although not shown, for

L/D = 1.58, the C_p curve dips negative but remains flat for 0.1 < z < 0.9. In

Figure 13, the x's are the source and sink. In each figure there are two vertical

lines passing through the source and sink; the vertical lines are located at

z = 0 and z = 1.

As L/D increases, it is apparent from the figure sequence that C_p at z = 0.5

becomes less negative and approaches zero. At L/D equal to 6, C_p is less than

3 per cent of the positive peak for the stagnation point. A laser turret installed

at z = 0 on a fuselage with L/D = 6 would experience freestream velocity within

1.5 per cent. Using equation (50) and the binomial expansion, one can show that

$$u = 1 - \frac{C_p}{2}$$ (52)

Application of equation (52) to the case of L/D = 6 gives u = 1.015.

309

The Boeing 707-320 has a fineness ratio of 10; and the French Caravelle, 10.4. The stretch DC-8 has L/D considerably more than 10. The Boeing 747SP, which is a standard 747 with a section of fuselage removed, has L/D near 6. Another wide body jet, the DC-10, has L/D near 8.6. The laser turret on the Airborne Laser Laboratory, ALL, is on a fuselage with L/D of 10, and the turret is located at nondimensional z = 0.3 approximately. Looking at Figure 17, one notes C_p is nearly zero at z - 0.3. Consequently, the turret should be experiencing near freestream velocity. (The preceding statement ignores interference effects of other components, e.g., wing.)

A potential flow solution provides insight to the effect of fuselage ends on the airflow likely to be present near a laser turret. For L/D = 6, a turret near z = 0.5 will have essentially freestream velocity. For L/D = 10, freestream conditions prevail in the interval 0.3 < z < 0.7.

Formulation of Subsonic Flow over a Laser Turret

For small perturbation flow, the potential equation as derived in Liepmann and Roshko [18] is

$$\pm \beta^2 \phi_{xx} + \phi_{rr} + \frac{1}{r} \phi_r + \frac{1}{r^2} \phi_{\theta\theta} = 0 \tag{53}$$

The (+) sign applies to subsonic flow; and the (-) sign, to supersonic flow. the definition of β is

$$\beta^2 = |1 - M_\infty^2| \tag{54}$$

The function φ is the perturbation potential yielding only the changes from the freestream velocity. Equation (53) is given in cylindrical coordinates which are appropriate for the cylindrical fuselage. A solution to equation (53) can be obtained using the separation of variables. For the flow field external to the fuselage

$$\phi(r,\theta,x) = A \cos n\theta \sin qx \, K_n(\beta qr) \tag{55}$$

310

where A is a constant, n is an integer, and q is to be determined. See Fuhs and Fuhs [2] for development of the solution in detail.

The turret shape is defined by

$$R(x,\theta) = R_0 + \epsilon X(x) T(\theta) \tag{56}$$

where $X(x)$ and $T(\theta)$ are functions. The height of the turret is ϵ as shown in Figure 11. As an example, a cosine shaped turret will be used. For a cosine shaped turret

$$X(x) = \frac{1}{2}(1 + \cos \frac{\pi x}{\ell}) \tag{57}$$

and

$$T(\theta) = \frac{1}{2}(1 + \cos f\theta) \tag{58}$$

Equations (58) and (59) apply for $|x| \leq \ell$ and $|\theta| \leq 2\pi/f$. Outside this region $R = R_0$. The quantity $1/f$ is the fraction of the 2π-circumference occupied by the turret, and ℓ is the length of the turret. For a cosine shaped turret, the appropriate Fourier series are

$$X(x) = \frac{\epsilon \ell}{2L} + \frac{\epsilon \ell}{L} \sum_{m=1}^{\infty} \frac{\sin m\pi\ell/L}{m\pi\ell/L} \frac{1}{1 - (m\ell/L)^2} \cos \frac{m\pi x}{L} \tag{59}$$

and

$$T(\theta) = \frac{1}{2f} + \frac{1}{f} \sum_{n=1}^{\infty} \frac{\sin n\pi/f}{n\pi/f} \frac{1}{1 - (n/f)^2} \cos n\theta \tag{60}$$

In equation (59) the spacing between periodic turrets on an infinitely long fuselage is L. The turret generated by equations (56), (59), and (60) is shown in Figure 11.

At the body surface for inviscid flow, there can be no flow through the wall. Mathematically this is expressed by

$$\vec{n} \cdot \vec{V} = 0 \qquad (61)$$

where $\vec{n}$ is a unit vector normal to an element of the surface and $\vec{V}$ is the vector representing the local fluid velocity. If one can express the shape of a body by an equation of the form $f(r,\theta,x) = 0$, then

$$\vec{n} = \vec{\nabla}f/|\vec{\nabla}f| \qquad (62)$$

Using the potential function for determining $\vec{V}$, the boundary condition at the body surface is

$$\vec{\nabla}\Phi \cdot \vec{\nabla}f = 0 \qquad (63)$$

where Φ is the full potential related to the perturbation potential by

$$\Phi = \phi + xU_{\infty} \qquad (64)$$

For small perturbation, equation (63) reduces to

$$\frac{\partial f}{\partial x} + \frac{\partial \Phi}{\partial r} = 0 \qquad (65)$$

Equation (65) is derived in Appendix A of reference [3].

Solutions for Subsonic Flow

In view of equations (56), (59), and (60), the potential function is assumed to have the form

$$\phi(r,\theta,x) = \sum_n \sum_m \phi_{nm}(r,\theta,x) \qquad (66)$$

Using appropriate nondimensional variables, ϕ_{nm} is found to be

$$\phi_{nm}(r,\theta,x) = -\frac{2A_{nm} \cos n\theta \sin \frac{m\pi x}{L} K_n(\beta m\pi r/L)}{\beta[K_{n+1}(\beta m\pi/L) + K_{n-1}(\beta m\pi/L)]} \qquad (67)$$

K_n is a Bessel function discussed in the book by Hildebrand [19]. The constant A_{nm} is given by

312

$$A_{nm} = - \frac{\varepsilon \ell}{fL} \left[\frac{1}{1 - (\ell m/L)^2} \frac{\sin(m\pi \ell/L)}{(m\pi \ell/L)} \right] \left[\frac{1}{1 - (n/f)^2} \frac{\sin(n\pi/f)}{(n\pi/f)} \right] \tag{68}$$

Combining equations (66) to (68), one has the complete perturbation potential equation. The perturbation velocities are calculated using $\vec{\nabla}\phi$; these velocities are shown explicitly in reference [3]. With velocities in nondimensional form, the pressure coefficient for axisymmetric flow is

$$C_p = - 2u - v^2 \tag{69}$$

Equation (69) can be evaluated, and the results inserted in equation (7) to calculate the phase distortion P.

Before discussing typical results for phase distortion, calculation of critical Mach will be presented. Equation (3) relates p/p_∞ to the pressure coefficient, C_p. Assume the flow is isentropic; this assumption permits use of the following relation between static pressure where the local Mach number is unity, p^*, and the static pressure at infinite distance from the turret, p_∞:

$$\frac{p^*}{p_\infty} = \left[\frac{2}{\gamma + 1} \left(1 + \frac{\gamma - 1}{2} M_\infty^2 \right) \right]^{\frac{\gamma}{\gamma - 1}} \tag{70}$$

Combining equations (3) and (70) establishes an equation for the critical pressure coefficient

$$C_p^* = \frac{2}{\gamma M_\infty^2} \left\{ \left[\frac{2}{\gamma + 1} \left(1 + \frac{\gamma - 1}{2} M_\infty^2 \right) \right]^{\frac{\gamma}{\gamma - 1}} - 1 \right\} \tag{71}$$

When C_p given by equation (69) equals C_p^*, the local velocity is sonic. Equations (69) and (71) were used to calculate the critical Mach numbers given in Table I.
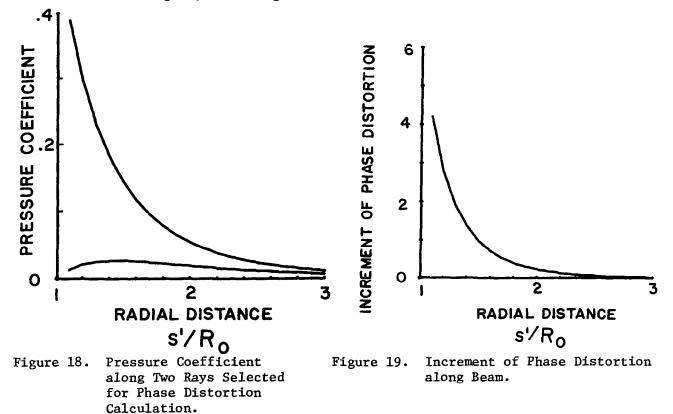
Typical Results

As an example, the phase distortion was calculated for a laser beam leaving the turret of Figure 11. The beam was pointed at an angle 90° to the axis of the fuselage and was symmetrically located relative to the turret. The beam radius was

$\ell/2$. The pressure coefficient and optical path length were calculated for a ray starting at $x = -\ell/2$ and for the reference ray at $x = 0$. The pressure coefficient along the two rays is shown in Figure 18. The values used in the calculation were as follows:

$$M_\infty = 0.62 \qquad R_0 = 1 \quad \text{meter} \qquad L = 5$$

$$\varepsilon = 0.35 \qquad \lambda = 3.8 \text{ microns} \qquad \theta = 0$$

$$\rho_\infty/\rho_{SL} = 1.0 \qquad \ell = 1.005 \qquad \kappa' = 0.00023$$

The quantity $\partial P/\partial(s'/R_0)$ was evaluated for the two rays specified above. The results are shown in Figure 19, which is a graph of increment of phase distortion as a function of radial distance s'. About one-half of the phase distortion occurs within a distance along the beam of approximately $0.35\ R_0$. Expressed in terms of turret height, ε, one-half of the phase distortion is generated within approximately one turret height.

The integrated phase distortion, which is the area under the curve, is 1.17. In terms of wavelengths, the integrated distortion is 1.17λ.

Figure 18. Pressure Coefficient along Two Rays Selected for Phase Distortion Calculation.

Figure 19. Increment of Phase Distortion along Beam.

TURRET ON A CIRCULAR CROSS SECTION FUSELAGE: SUPERSONIC FLOW

The potential flow equation for supersonic flow is equation (53) with use of the (-) sign. Once again the turret shape is illustrated by Figure 11. A more general formulation for turret geometry is developed in this section.

Turret Geometry

The function X(x) of equation (56) is a polynomial

$$X(x) = 1 + \sum_{k=1}^{K} \tilde{a}_k x^k \tag{72}$$

Likewise the function T(θ) of equation (56) is another polynomial

$$T(\theta) = 1 + \sum_{j=2,4,}^{P} \tilde{b}_j \theta^j \tag{73}$$

Note that only even powers of θ are used since the turret is symmetric in the θ-direction. As before, ε is the height of the turret at $x = \theta = 0$. Each term in the polynomial is expanded separately as a Fourier series [20].

$$x^k = \sum_{m=0}^{\infty} a_{mk} \cos \frac{m\pi x}{L} + b_{mk} \sin \frac{m\pi x}{L} \tag{74}$$

Hence

$$X(x) = \sum_{k=1}^{K} a_k \left(\sum_{m=0}^{\infty} \tilde{a}_{mk} \cos \frac{m\pi x}{L} + b_{mk} \sin \frac{m\pi x}{L} \right) \tag{75}$$

In a similar manner

$$\theta^j = \sum_{n=0}^{\infty} a_{nj} \cos n\theta \tag{76}$$

Consequently

$$T(\theta) = \sum_{j=2,4,}^{p} \tilde{b}_j \left(\sum_{n=0}^{\infty} a_{nj} \cos n\theta \right) \qquad (77)$$

The Fourier coefficients are as follows:

$$a_{mk} = \frac{\ell^k}{m\pi} [(-1)^k + 1] \sin \frac{m\pi\ell}{L} - \frac{kL}{m\pi} b_{m,k-1} \qquad (78)$$

$$b_{mk} = -\frac{\ell^k}{m\pi} [(-1)^{k+1} + 1] \cos \frac{m\pi\ell}{L} + \frac{kL}{m\pi} a_{m,k-1} \qquad (79)$$

Equations (78) and (79) are recursion relations. To start the sequence one

needs a_{0k} and b_{0k} which are

$$a_{0k} = \frac{[(-1)^k + 1]\ell^{k+1}}{2L(k+1)} \qquad (80)$$

and

$$b_{0k} = 0 \qquad (81)$$

Also both $a_{m,-1}$ and $b_{m,-1}$ are zero. Beginning with k = 0, the Fourier

coefficients for any order polynomial can be obtained using equations (78) to

(81). If k is an even number, then b_{mk} is zero. If k is an odd number, then

a_{mk} is zero.

Equations (72) through (81) define a turret of length 2ℓ which is periodic

every x = 2L. In the circumferential direction, the turret is positioned

between $-\theta_t \le \theta \le \theta_t$, where θ_t defines the boundary of the turret. To evaluate

equation (77), one needs a_{nj}. Equations (78) to (81) can be used to determine a_{nj}

by making the following substitutions:

$$m \rightarrow n \qquad\qquad L \rightarrow \pi$$

$$k \rightarrow j \qquad\qquad \ell \rightarrow \theta_t$$

Note that j has only even values.

The coefficients $\overset{\sim}{a_k}$ and $\overset{\sim}{b_j}$ will be varied; however, because of the geometry not all coefficients may be independent. Due to equations (56), (72), and (73), the turret height at $x = \theta = 0$ is always ε. To have a continuous surface for the fuselage, $X(x) = 0$ for $|x| = \ell$; also, $T(\theta) = 0$ for $|\theta| = \theta_t$. In addition, conditions may be imposed such that $dX/dx = 0$ at $|x| = \ell$, etc.

For each boundary condition imposed, one coefficient of the polynomial is eliminated as an independent variable. The coefficients which are not used to satisfy boundary conditions can be used as design variables. In a companion paper [21], the design variables are selected so as to optimize phase distortion.

Solution to Potential Equation for Supersonic Flow

Once again separation of variables is used to solve equation (53). The solution has the form

$$\phi(r,\theta,x) = R(r)\Theta(\theta)X(x) \tag{82}$$

where

$$R(r) = AJ_n(\beta qr) + BY_n(\beta qr) \tag{83}$$

$$\Theta(\theta) = C \sin n\theta + D \cos n\theta \tag{84}$$

$$X(x) = E \sin qx + F \cos qx \tag{85}$$

Both J_n and Y_n are Bessel functions discussed by Hildebrand [19]. For symmetry with respect to $\theta = 0$, C is zero. Since both J_n and Y_n are finite for large r, neither A nor B can be set equal to zero. In contrast to the subsonic flow solution, the supersonic flow solution has one additional constant to be determined. Matching waves in the far field permits evaluation of the additional constant [22]. For a simple cosine wavy wall on a cylinder, the potential equation has the form as derived by Fuhs [23]

$$\phi(r,x) = A[(\sin \alpha x - \cos \alpha x)Y_0(\alpha\beta r) + (\sin \alpha x + \cos \alpha x)J_0(\alpha\beta r)] \tag{86}$$

The constant A is related to the amplitude of the cosine wavy wall. Equation (86) implies an eigenvalue given by

$$Y_1(\alpha\beta R_0) = - J_1(\alpha\beta R_0) \tag{87}$$

The wavenumber of the wavy wall is α.

The requirement for no flow through the turret boundary is given by equation (65). For the turret of Figure 11, the boundary condition becomes

$$\frac{v}{U} = \left.\frac{\partial R}{\partial x}\right)_{r=R_0} = \left.\frac{1}{U}\frac{\partial \phi}{\partial r}\right)_{r=R_0} \tag{88}$$

The surface of the turret is given by

$$R(\theta,x) = R_0 + \sum_n \sum_m \left[A_{nm} \cos \frac{m\pi x}{L} + B_{nm} \sin \frac{m\pi x}{L}\right] \cos n\theta \tag{89}$$

Based on equation (86), the potential function is assumed to have the form

$$\phi(r,\theta,x) = U_\infty x + \sum_n \sum_m \phi_{nm} \tag{90}$$

where

$$\phi_{nm}(r,\theta,x) = \lambda_{nm} \cos n\theta \left[\left(\sin \frac{m\pi x'}{L} - \cos \frac{m\pi x'}{L}\right)Y_n\left(\frac{\beta m\pi}{L} r\right)\right.$$

$$\left. + \left(\sin \frac{m\pi x'}{L} + \cos \frac{m\pi x'}{L}\right)J_n\left(\frac{\beta m\pi}{L} r\right)\right] \tag{91}$$

Equation (87) establishes an eigenvalue, which is the root of equation (87). For a Fourier series, the wavenumber α is determined by the series. The flight Mach number determines β. Hence R_0 is not arbitrary. As a result one must introduce an eigenvalue cylinder which has the same wavenumber as the cylinder required by the Fourier series; however, the eigenvalue cylinder has a different radius.

Further, the eigenvalue cylinder is shifted in phase. The equation for a cosine shaped eigenvalue cylinder is

$$R_{nm}(\theta,x) = R_{mn} + \epsilon_{mn} \cos n\theta \cos \frac{m\pi x'}{L} \tag{92}$$

The boundary condition for the eigenvalue cylinder is

$$\left.\frac{\partial \phi_{nm}}{\partial r}\right)_{r=R_{nm}} = \frac{\partial R_{nm}}{\partial \chi} \tag{93}$$

The phase shift, x_{nm}, is given by

$$x' = x + x_{nm} \tag{94}$$

Carefully note that $R_{nm}(\theta,x)$ and ϕ_{nm} are formulated with x' whereas R(θ,x) is in terms of x.

Consider first the cosine wavy wall defined by equation (92). Use of the boundary condition of equation (93) gives the eigenvalue equation

$$\frac{\beta m\pi R_{nm}}{L} [Y_{n+1}(C_m) - J_{n+1}(C_m)] - n[Y_n(C_m) - J_n(C_m)] = 0 \tag{95}$$

where

$$C_m = \frac{\beta \pi m R_{nm}}{L} \tag{96}$$

There is only one value of R_{nm} which satisfies equation (95); hence equation (95) provides a method to calculate R_{nm} in equation (92).

From the boundary condition of equation (93), one finds

$$\epsilon_{nm} = \frac{\lambda_{nm}\left\{ C_m[Y_{n+1}(C_m) + J_{n+1}(C_m)] - n[Y_n(C_m) + J_n(C_m)] \right\}}{\dfrac{m\pi R_{nm}}{L}} \tag{97}$$

Using the boundary condition for the turret as given by equation (88), the phase shift, x_{nm}, can be determined

$$\tan \frac{m\pi x_{nm}}{L} = \frac{D_{nm} - E_{nm}}{D_{nm} + E_{nm}} \tag{98}$$

where D_{nm} and E_{nm} are defined as

$$D_{nm} = -\frac{\beta m\pi}{L} Y_{n+1}\left(\frac{\beta\pi m R_0}{L}\right) + \frac{n}{R_0} Y_n\left(\frac{\beta\pi m R_0}{L}\right) \tag{99}$$

and

$$E_{nm} = -\frac{\beta m\pi}{L} J_{n+1}\left(\frac{\beta m\pi R_0}{L}\right) + \frac{n}{R_0} J_n\left(\frac{\beta\pi m R_0}{L}\right) \tag{100}$$

Continuing with the boundary condition for the turret, define

$$a_{nm} = D_{nm} + E_{nm} \tag{101}$$

and

$$b_{nm} = D_{nm} - E_{nm} \tag{102}$$

The amplitude of ϕ_{nm} term, which is λ_{nm}, is related to A_{nm} of equation (89) by

$$\lambda_{nm} = -\frac{m\pi A_{nm}}{L[a_{nm}^2 + b_{nm}^2]^{1/2}} \tag{103}$$

The value of A_{nm} is determined by turret shape. Combining equations (91), (94), (98), and (99) through (103), one obtains

$$\phi_{nm}^c(r,\theta,x) = -\frac{(m\pi/L)A_{nm}\cos n\theta}{a_{nm}^2 + b_{nm}^2}\Bigg\{ (a_{nm} + b_{nm})\sin\frac{m\pi x}{L} Y_n\left(\frac{\beta m\pi r}{L}\right)$$

$$- (a_{nm} - b_{nm})\cos\frac{m\pi x}{L} Y_n\left(\frac{\beta m\pi r}{L}\right)$$

$$+ \left[(a_{nm} - b_{nm})\sin\frac{m\pi x}{L} + (a_{nm} + b_{nm})\cos\frac{m\pi x}{L}\right]J_n\left(\frac{\beta m\pi r}{L}\right)\Bigg\} \tag{104}$$

Following a similar procedure for the sine shaped wavy wall, one finds

$$\phi^s_{nm}(r,\theta,x) = -\frac{(m\pi/L)B_{nm}\cos n\theta}{a^2_{nm} + b^2_{nm}} \left\{ -(a_{nm} + b_{nm}) \cos \frac{m\pi x}{L} Y_n(\frac{\beta m\pi r}{L}) \right.$$

$$+ (a_{nm} - b_{nm}) \sin \frac{m\pi x}{L} Y_n(\frac{\beta m\pi r}{L})$$

$$\left. - [(a_{nm} - b_{nm}) \cos \frac{m\pi x}{L} - (a_{nm} + b_{nm}) \sin \frac{m\pi x}{L}] J_n(\frac{\beta m\pi r}{L}) \right\} \tag{105}$$

The combined potential equation is

$$\phi(r,\theta,x) = U_\infty x + \sum_n \sum_m (\phi^c_{nm} + \phi^s_{nm}) \tag{106}$$

Equation (106) can be used to determine the velocity components. With the velocity components, equation (69) can be evaluated for the pressure coefficient, C_p. In turn, the pressure coefficient can be inserted into equation (7) to determine the phase distortion, P.

Results of a Sample Calculation

The flow over a cosine shaped turret was determined. The turret was defined by equations which approximate a cosine

$$X(x) = 1.0 - 0.5(x/\ell)^2 + 0.0625(x/\ell)^4 \tag{107}$$

and

$$T(\theta) = 1.0 - 1.82(\theta/\theta_t)^2 + 0.0832(\theta/\theta_t)^4 \tag{108}$$

The Mach number was $M_\infty = 2.0$, $\epsilon = 0.2$, $\ell = 2R_0$, and $\theta_t = 60^\circ$.

Figure 20 shows the phase distortion map for the case being considered here. The distortion is almost pure tilt.
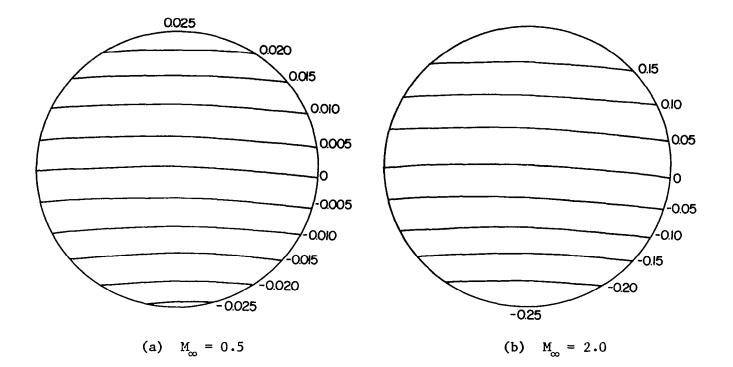
Figure 20. Map of Phase Distortion. Azimuth $0°$; Elevation $45°$; Mirror Radius = $R_0/20$.

CONCLUSIONS

Laser turrets may be classified as blunt or small perturbation depending on maximum slope of the turret surface. Analytical models were developed for both categories of turrets.

As an example of a blunt laser turret, the flow over a hemispherical turret was solved using Janzen-Rayleigh expansion technique. Terms to the second order were obtained and were used to calculate the phase distortion. At the critical Mach number for a hemispherical turret, the phase distortion was several wavelengths. The phase distortion varied from a positive focus for $0°$ elevation to combined focus and tilt at intermediate elevations and to negative focus for $90°$ elevation. The distortion can be expressed in terms of Zernike polynomials.

A versatile analytical model was developed for a laser turret on an infinitely long circular cylinder. The laser turret is described by a two-dimensional Fourier series using the solution for the flow over a wavy wall on a cylinder. The turret can have any shape subject to the constraint that the turret is a small perturbation in the flow. Both subsonic and supersonic solutions were obtained.

End effects were examined. For a fuselage with length to diameter ratio of 6.0, the laser turret mounted at the midpoint of the fuselage would experience freestream velocity with 1.5 per cent. For an aircraft with L/D of 10, such as ALL, any location between $z/D = 0.3$ to $2/D = 0.7$ would have freestream conditions.

The analytical model permits calculation of critical Mach number for the turret. The critical Mach number is important because of the change from linearized subsonic flow solution to nonlinear transonic flow.

For the subsonic case, the maximum observed distortion was a fraction of wavelength. Similar results were found at Mach 2.

The supersonic flow solution has eigenvalues which require introduction of an eigenvalue cylinder. A cylinder of arbitrary radius cannot yield a satisfactory solution. A cylinder slightly smaller can satisfy the boundary conditions and becomes the eigenvalue cylinder. For large radial distances from the cylinder, the solution approaches that of a planar wavy wall.

In addition to useful calculations for laser turrets, the analytical models are useful for reconnaissance aircraft using cameras and cruise missiles using celestial navigation.

REFERENCES

1. P. J. Klass, "Special Report: Laser Weapons. Advanced Weaponry Research Intensifies," *Aviation Week and Space Technology*, Vol. 103, No. 7, August 18, 1975.

2. Anonymous, "High Energy Laser Development," *International Defense Review*, Vol. 12, No. 3, p. 316, 1979.

3. A. E. Fuhs and S. E. Fuhs, "Phase Distortion at High Subsonic Mach Numbers for a Small Perturbation Laser Turret," *Proceedings of Electro-optical Systems Design Conference - 1976*, New York, pp. 9-19, published by Industrial and Scientific Conference Management, Inc., 222 W. Adams St., Chicago, IL, 60606.

4. A. E. Fuhs, "Potential Flow: Nonlinear Compressible Flow," Lecture 3B, Short Course on Laser Aerodynamics, presented April 11-22, 1977, at AF Weapons Laboratory, Kirtland, AFB, NM.

5. M. Van Dyke, *Perturbation Methods in Fluid Mechanics*, Academic Press, New York, 1964.

6. T. Hsieh, "Hemisphere-Cylinder in Transonic Flow, $M_\infty = 0.7 - 1.0$," *AIAA Journal*, 13, pp. 1411-1413, 1975.

7. T. Hsieh, "Hemisphere-Cylinder in Low Supersonic Flow," *AIAA Journal*, 13, pp. 1551-1552, 1975.

8. H. W. Liepmann and A. E. Puckett, *Introduction to Aerodynamics of a Compressible Fluid*, John Wiley and Sons, New York, 1947. See Chapter 10.

9. K. Oswatitsch, *Gas Dynamics*, Academic Press, New York, 1956. See pages 328-334.

10. Lord Rayleigh, "On the Flow of Compressible Fluid Past an Obstacle," *The London, Edinburgh, and Dublin Philosophical Magazine and Journal*, Sixth Series, Vol. 32, No. 187, July, 1916.

11. M. Born and E. Wolf, *Principles of Optics*, Pergamon Press, New York, 1964.

12. C. B. Hogge and R. R. Butts, "Frequency Spectra for the Geometric Representation of Wavefront Distortions Due to Atmospheric Turbulence," *IEEE Transactions on Antennas and Propagation*, Vol. AP-24, pp. 144-154, 1976.

13. A. E. Fuhs and S. E. Fuhs, "Phase Distortion due to Airflow over a Hemispherical Laser Turret," Naval Postgraduate School Report NPS-69FU76101, September, 1976.

14. A. E. Fuhs, "Distortion of Laser Turret Optics Due to Aircraft Mainstream Flow," *Journal of the Optical Society of America*, 66, p. 1137, 1976.

15. L. M. Milne-Thompson, Theoretical Hydrodynamics, Macmillan Co., New York, Fourth Edition, 1960.

16. H. Lamb, Hydrodynamics, Dover Publications, New York, Sixth Edition, 1945.

17. K. Karamcheti, Principles of Ideal-Fluid Aerodynamics, John Wiley and Sons, New York, 1966.

18. H. W. Liepmann and A. Roshko, Elements of Gasdynamics, John Wiley and Sons, New York, 1957.

19. F. B. Hildebrand, Advanced Calculus for Engineers, Prentice-Hall, Inc., New York, 1949.

20. A. E. Fuhs and G. N. Vanderplaats, "Aero-optics: Polynomial Representation of Laser Turret in Subsonic Flow and Completion of Formulation of Supersonic Flow," Progress Report 77-1 to AFWL, 10 November 1976.

21. G. N. Vanderplaats, A. E. Fuhs, and G. A. Blaisdell, "Optimized Laser Turret for Minimum Phase Distortion," Paper, This Conference.

22. A. E. Fuhs, "Aero-optics," Progress Report No. 2 to AFWL, 20 November 1975.

23. A. E. Fuhs, "Aero-optics," Progress Report No. 1, to AFWL, 6 September 1975.